Biomedicine & Pharmacotherapy 161 (2023) 114486

Contents lists available at ScienceDirect

Biomedicine & Pharmacotherapy

journal homepage: www.elsevier.com/locate/biopha

Discovery of drug targets and therapeutic agents based on drug repositioning to treat lung adenocarcinoma

Occam Kelly Graves [a,1], Woonghee Kim [b,1], Mehmet Özcan [b], Sajda Ashraf [c], Hasan Turkez [c], Meng Yuan [b], Cheng Zhang [b], Adil Mardinoglu [b,d,*], Xiangyu Li [b,e,f,*]

[a] Harvey Mudd College, Claremont, CA 91711, USA
[b] Science for Life Laboratory, KTH-Royal Institute of Technology, Stockholm SE-17165, Sweden
[c] Trustlife Labs, Drug Research & Development Center, 34774 Istanbul, Turkey
[d] Centre for Host-Microbiome Interactions, Faculty of Dentistry, Oral & Craniofacial Sciences, King's College London, London SE1 9RT, UK
[e] Bash Biotech Inc, 600 West Broadway, Suite 700, San Diego, CA 92101, USA
[f] Guangzhou Laboratory, Guangzhou 510005, China

ARTICLE INFO

Keywords:
Lung adenocarcinoma
Co-expression network
Target identification
Drug repositioning

ABSTRACT

Background: Lung adenocarcinoma (LUAD) is the one of the most common subtypes in lung cancer. Although various targeted therapies have been used in the clinical practice, the 5-year overall survival rate of patients is still low. Thus, it is urgent to identify new therapeutic targets and develop new drugs for the treatment of the LUAD patients.

Methods: Survival analysis was used to identify the prognostic genes. Gene co-expression network analysis was used to identify the hub genes driving the tumor development. A profile-based drug repositioning approach was used to repurpose the potentially useful drugs for targeting the hub genes. MTT and LDH assay were used to measure the cell viability and drug cytotoxicity, respectively. Western blot was used to detect the expression of the proteins.

Findings: We identified 341 consistent prognostic genes from two independent LUAD cohorts, whose high expression was associated with poor survival outcomes of patients. Among them, eight genes were identified as hub genes due to their high centrality in the key functional modules in the gene-co-expression network analysis and these genes were associated with the various hallmarks of cancer (*e.g.*, DNA replication and cell cycle). We performed drug repositioning analysis for three of the eight genes (*CDCA8*, *MCM6*, and *TTK*) based on our drug repositioning approach. Finally, we repurposed five drugs for inhibiting the protein expression level of each target gene and validated the drug efficacy by performing *in vitro* experiments.

Interpretation: We found the consensus targetable genes for the treatment of LUAD patients with different races and geographic characteristics. We also proved the feasibility of our drug repositioning approach for the development of new drugs for disease treatment.

1. Introduction

Lung cancer is the most lethal cancer worldwide, causing more than 1.7 million deaths in 2020 [1]. Lung adenocarcinoma (LUAD) is the most prevalent histologic subtype in lung cancer, and accounts for half of all lung cancer deaths [2]. LUAD has a strong association with smoking history, while it also showed an increasing occurrence in non-smokers [2]. Patients with localized and early-stage tumor receive standard surgical resection, but the majority of patients are usually diagnosed at an advanced stage and recommended the conventional therapies including chemoradiotherapy, targeted therapy and immunotherapy. Various mutations in genes *EGFR*, *ALK*, *KRAS*, *ROS1*, *BRAF*,

Abbreviations: LUAD, Lung adenocarcinoma; CDR, Computational drug repositioning; TPM, Transcripts per million; OS, overall survival; GO, Gene Ontology.

* Corresponding authors at: Science for Life Laboratory, KTH-Royal Institute of Technology, Stockholm SE-17165, Sweden
E-mail addresses: occamkg@gmail.com (O.K. Graves), woonghee.kim@scilifelab.se (W. Kim), mehmet.ozcan@scilifelab.se (M. Özcan), Sajda.ashraf@trustlifelabs.com (S. Ashraf), hturkez@atauni.edu.tr (H. Turkez), meng.yuan@scilifelab.se (M. Yuan), cheng.zhang@scilifelab.se (C. Zhang), adilm@scilifelab.se (A. Mardinoglu), xiangyu.li@scilifelab.se (X. Li).

[1] These authors contributed equally to this paper.

https://doi.org/10.1016/j.biopha.2023.114486
Received 21 December 2022; Received in revised form 20 February 2023; Accepted 7 March 2023
Available online 10 March 2023

NTRK1/2/3, *MET*, *RET*, and *ERBB2* are observed in LUAD patients with relatively high coverages and these genes are involved in the molecular testing for patients' targeted therapy recommendation in clinical practice [3]. For instance, the first-line treatment for patients with *EGFR* activating mutations includes tyrosine kinase inhibitors osimertinib, erlotinib, afatinib, gefitinib and dacomitinib. Despite these different therapy regimens, 5-year overall survival rate ranges from 4 % to 17 % depending on different tumor stages and regions [4]. Thus, there is need to discover new drug targets and develop effective drugs for LUAD treatment, and thus improve the survival outcomes of patients.

Numerous studies have focused on the identification of biomarker genes based on the bioinformatics analysis of transcriptomics profiles of LUAD patients [5–13]. These studies validated the importance of the identified biomarkers by proving the prognostic value of these genes or linking these genes with some meaningful tumor hallmarks, *e.g.*, immune infiltration, cell differentiation or glycolysis. However, none of these studies attempted to find the potential drug candidates for targeting the marker genes. Computational drug repositioning (CDR), aims to identify new uses of existing drugs based on data driven analysis, has now been widely used in drug discovery for development of treatments for different human diseases. Traditional drug discovery utilizes a *de novo* design approach, which requires high cost and many years of drug development before it reaches to the market. In contrast, CDR can dramatically decrease the overall cost, time duration and development risks of bringing the drug to market because it aims to reuse the clinical drugs or compounds under preclinical investigation, Moreover, the safety, pharmacokinetic profiles, formulation development and even bulk manufacturing of these drugs have been well-characterized in early medical investigation and these processes can be therefore by-passed. The recent meaningful examples were observed from the current Covid-19 outbreak. JAK inhibitor baricitinib and antiviral medicine paxlovid (nirmatrelvir /ritonavir) have been authorized for emergency use by FDA for the treatment of Covid-19 patients, which are previously used for treatment of rheumatoid arthritis and HIV infection, respectively. CDR, including various data-driven approaches such as drug/-protein structure-based similarity analysis and gene expression profile-based signature matching or pathway modulating, provides a systematic way to discover all possible pairs between the drugs and disease targets or pathways [14–17]. It also provides information about the mechanisms of action of a drug in disease treatment. Especially, profile-based CDR does not rely on the prior knowledge, and it increases the ability to discovery new drug-disease-target pairs [18]. It has been reported that drug repositioning accounts for approximately 30 % of the newly FDA-approved drugs and vaccines in recent years [19,20]. Huang et al. identified 1597 LUAD-related genes and applied a network-overlap and -distance based drug repositioning method to detect the potential drug candidates for targeting these genes [21]. However, this study did not provide any experimental validation for the drug efficacy. Bastiani et al. [22] and Kwon et al. [23] employed a profile-based drug repositioning approach by mapping the drug-induced and LUAD-associated gene expression profiles based on the hypothesis that a drug is considered to have a therapeutic worth if it can reverse the disease-associated molecular dysregulation. However, a drug identified by this method is supposed to have multiple gene targets, mixed with driver oncogenes and passenger genes, which limits the understanding and validation of the drug mechanism of action. To solve this problem, we recently proposed a computational drug repositioning method to predict the drugs that can target a specific gene instead of general regulation of a set of disease-related genes [15]. Moreover, we have validated the feasibility of our drug repositioning approach for the treatment of kidney and liver cancers as well as non-alcoholic fatty liver disease [15,24,25].

In this study, we identified the hub genes that drives the LUAD development and repurposed the promising drugs that can target these genes. First, we identified consensus prognostic genes in two independent LUAD cohorts based on survival analysis. Secondly, we constructed the cohort-specific gene co-expression networks based on their transcriptomics profiles and identified a set of gene modules associated with the patients' prognoses. Further, we identified potential the promising drugs for these targets and validated the drug efficacy by performing *in vitro* cell line experiments.

2. Methods

The whole study design was shown in Fig. 1. To identify the therapeutic target genes and effective drugs for targeting these targets, we performed four steps of systems biology-based analyses based on the RNA-seq profiles of two independent LUAD cohorts. Step 1. Identify the prognostic genes by survival analysis. Step 2. Find the central prognostic genes based on the gene co-expression network analysis. Step 3. Rank the drugs based on a profile-based drug repositioning approach. Step 4. Validate the drug efficacy using an *in vitro* model. The methodology was described in detail as below.

2.1. Data pre-processing

The metadata and raw RNA-seq data of 497 LUAD patients from the TCGA cohort were downloaded from the GDC data portal (https://portal.gdc.cancer.gov/) [26]. Another independent cohort is from 199 non-small cell lung cancer patients surgically treated during 2006–2010 at the Uppsala University Hospital, Uppsala, Sweden (NCBI SRA database: SRP074349) [27,28]. From this cohort, we only used the RNA-seq data of 105 LUAD patients whose survival information was available. For both datasets, count and transcripts per million (TPM) values of transcripts were quantified by Kallisto based on the human reference genome Ensembl V103 [29]. Only protein-coding transcripts were filtered for further analysis. The sum count or TPM value of different alternative splicing transcripts from a gene was used as the gene expression value of this gene. Moreover, the genes with average TPM values > 1 were analyzed in this study.

2.2. Survival analysis

Cox proportional hazard regression was used to evaluate the association between gene expression levels and patients' overall survival (OS) based on the 'coxph' function from the R package 'survival' [30]. P-value < 0.01 was used to identify the significantly prognostic genes.

2.3. Functional enrichment analysis

The 'enrichGO' function from the R package 'clusterProfiler' (version 4.2.2) was used for the Gene ontology (GO) enrichment analysis, which detected the significantly enriched GO terms based on the hypergeometric distribution [31]. The 'org.Hs.eg.db' database was used as the GO term source (version 3.14.0). GO terms with FDR < 0.05 were used for further analysis. P-values were adjusted based on the Benjamini-Hochberg method.

2.4. Gene Co-expression network analysis

Based on the TPM values of genes, we employed the Spearman correlation to calculate the association of all possible gene pairs across all tumor samples in each cohort. Then, we constructed the gene co-expression network by extracting the gene-to-gene links ranked within top 1 % based on the highest correlation coefficients in each cohort. Then, a random walks-based algorithm, named Walktrap, was used to identify the gene modules with high transitivity [32]. The function "cluster_walktrap" in R package "igraph" was used to implement the Walktrap algorithm. Unweighted edges were used for community detection (weights=NULL) and the default settings recommended by this function were used for other parameters. Modules with more than 50 genes and clustering coefficients higher than 0.5 were used for further analysis. Clustering coefficient ranges from 0 and 1, and value

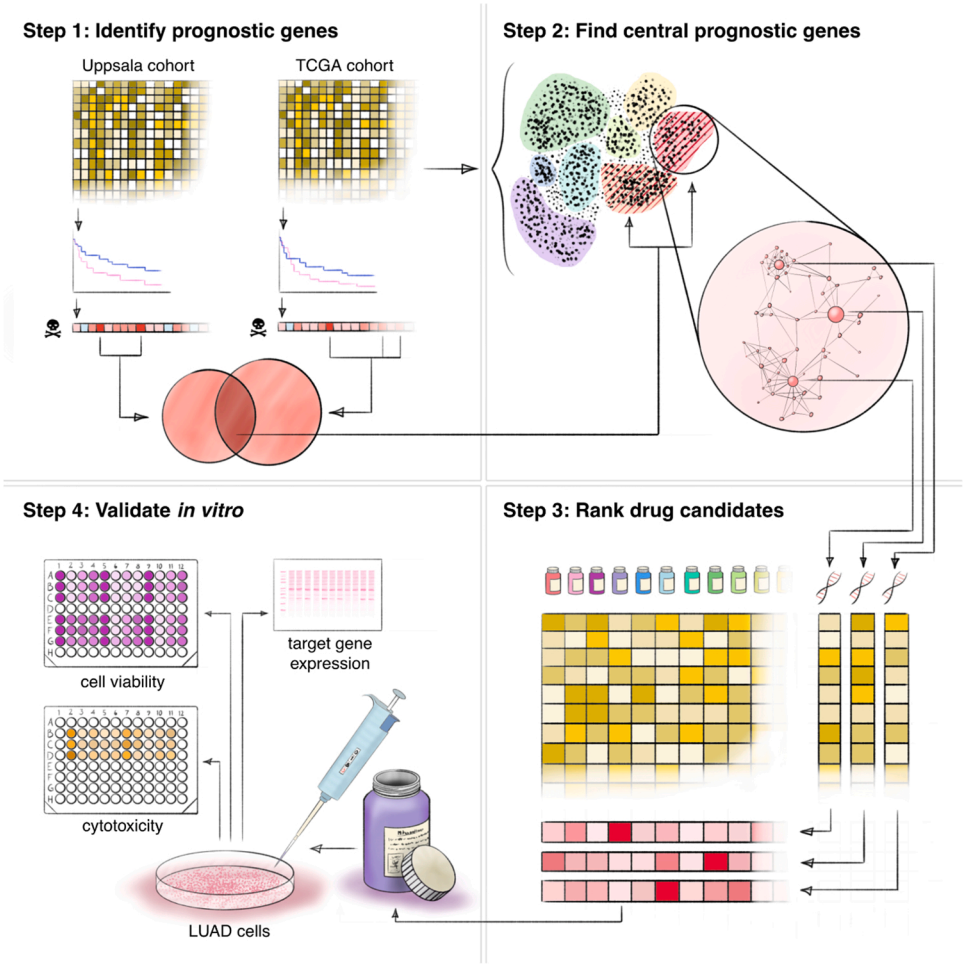

Fig. 1. Study design for the therapeutic target identification and drug repositioning for LUAD. Step 1. We identified a set of consistently prognostic genes based on the gene expression profiles of two independent LUAD cohorts and observed that the expression levels of these genes may indicate the survival outcomes of LUAD patients. Step 2. We constructed the gene co-expression network analysis in each of the two cohorts and identified the key gene modules that were also associated with patients' survival outcomes. Further, the central prognostic genes were identified based on the topology analysis of these modules, which were denoted as the druggable targets. Step 3. We applied a profile-based drug repositioning approach and repositioned the drugs that can potentially inhibit the protein expression levels of these target genes. Step 4. We tested the drug toxicity and validated the drug efficacy using an *in vitro* model.

higher than 0.5 is a commonly used cutoff which indicates that the partitions have a good cluster tendency and the genes involved in each module show a proper connectivity [33]. Degree, closeness, and betweenness values of genes were calculated in each module based on the R package 'igraph'.

2.5. Concordance analysis

The accumulative hypergeometric model was used to determine whether two lists of prognostic genes had a significant overlap as previously described [15]. This model was also used to test to determine whether the genes involved in a module had a significant overlap with the prognostic genes. Jaccard indices were calculated as the size of the overlapped genes divided by the size of the union of two lists of genes.

2.6. Essential scores of genes

The essential scores of genes in 50 LUAD cell lines were obtained from the DepMap Portal (https://depmap.org/portal/), which were calculated based on the CRISPR-Cas9 essentiality screens while accounting for the copy number-specific effect [34]. The score of a gene indicates the essentiality of this gene for cancer cell proliferation and survival after knockout of this gene by CRISPR-Cas9 technology. A more negative score indicates that the gene is more essential.

2.7. Drug repositioning for target genes

We applied our previously proposed drug repositioning approach to identify the potential promising drugs that can inhibit the target genes [15,24]. This method hypothesizes that a drug is considered to have an inhibitory effect on the expression of a target gene if this drug leads to a wide perturbation on the gene expression landscape in tumor cells which is similar to the effect of the knockdown of this target gene. The shRNA gene knockdown and drug perturbed transcriptomic gene signature profiles (level 5) of two LUAD cell lines A549 and HCC515 were downloaded from the Expanded CMap LINCS Resource (version 2020, https://clue.io/data/CMap2020#LINCS2020). The level 5 data provides the replicate-collapsed Z-scores, representing a consensus biological response of transcriptomics to the perturbation of drug treatment or gene knockdown derived from different replicates [35]. We performed the drug repositioning analysis for *CDCA8*, *MCM6*, and *TTK* since these genes had the available gene knockdown transcriptomic signature profiles. Each gene was knocked down by three different shRNAs, thus we obtained three gene knockdown perturbed signature profiles for each gene in both A549 and HCC515 cell lines. Meanwhile, we obtained 53,827 drug-perturbed signature profiles associated with 13,945 unique drugs with different dosages and treatment durations in A549 cell line, and 16,133 drug-perturbed signature profiles associated with 5890 unique drugs in HCC515 cell line.

In brief, there were four steps in the drug repositioning analysis. First, for a given gene, we created a drug-shRNA matrix by computing the Spearman correlation between this gene knockdown and drug treatment perturbed signature profiles in each cell line. In this matrix, each row represents a drug perturbagen with a specific dosage and treatment duration, and each column represents a gene knockdown with a specific shRNA. Second, we simplified the drug-shRNA matrix by selecting the optimal drug and shRNA perturbagens. A drug was added to the cells with different dosages and treatment durations in the CMap

experimental setting. To maximize the drug effect, we only kept a unique and optimal dosage/duration which showed the highest correlation coefficients with each shRNA perturbagen for each drug. Similarly, a gene was knocked down by three different shRNAs. To maximize the gene knockdown effect, we only kept an optimal shRNA perturbagen for each gene, which showed the highest mean correlation coefficient across all drugs. After optimization, each coefficient in the drug-shRNA matrix represents the similarity between the effects induced by a specific drug treatment (row) and a specific gene knockdown (column). Higher coefficient value means high possibility of the inhibitory effect of a drug on its target gene. Third, we merged the drug-shRNA matrices from the two cell lines by extracting the common drugs. Drugs that were not presented in both cell lines were excluded. Finally, for each gene, the top five drugs with the highest mean coefficients from the two cell lines were selected as the most effective drugs. Meanwhile, the coefficients in both cell lines should be greater than 0.4 which was an empirical cutoff based on our previous *in vitro* experimental validation [15,25].

2.8. Cell culture, MTT, and LDH assay

A549 cells were obtained from ATCC and cultured with culture medium (D0819 DMEM 10 % FBS 1% penicillin/streptomycin) at 37 °C. Cell viability was measured using an MTT assay. MTT ((3-[4,5-dimethylthiazol-2-yl]−2,5-diphenyltetrazolium bromide) (1×), at 5 mg/ml) was added for 1 h and formazan was dissolved with DMSO (dimethyl sulfoxide). Optical density at a wavelength of 570 nm was measured using a microplate reader (Hidex plate reader) to quantify the relative number of living cells. To determine treatment concentrations, cells were treated with serially diluted drugs until a concentration that reduced cell viability by around 50 %. As a result, 10 μM for CGP-60474 (MedChemExpress, HY-11009), 10 μM for wortmannin (Sigma, W1628) and 100 nM mitoxantrone (Selleckchem, NSC-301739) were used. Cells were treated with the drugs at their designated concentrations for two days.

Cytotoxic effect on the cells was measured with lactate dehydrogenase (LDH) assays that were performed in triplicates at the same concentrations as selected for the MTT assays following the LDH kit procedure (Abcam Cat# ab65393). 30 min after LDH (Abcam Cat# ab65393) administration, optical density at a wavelength of 450 nm was measured using a microplate reader (Hidex plate reader) to quantify the relative LDH activity which was released into the media *via* the drug's cytotoxic effect.

To normalize the quantification results, the mean negative control (untreated cells) reading was subtracted from each reading and then each was divided by the mean positive control (Cell Lysis Solution) reading minus the mean negative control reading.

2.9. Western blotting

Triplicates of drug treatments at the same concentrations as selected for the MTT assays were prepared for the Western blots. Whole cell lysate was extracted with CelLytic M (C2978, Sigma-Aldrich) lysis buffer. The protein content of each sample was measured using a Bradford assay and each sample was prepared for Western blotting using 2x Laemmli buffer. Electrophoresis was run at 150 V for 40 min and membrane transfer was performed with the Trans-Blot Turbo Transfer System (Biorad). PVDF membranes were blocked for 30 min with 5 % skim milk and TBST (Tris Buffered Saline with 0.2 % Tween 20) and then treated overnight on a shaker plate at 4 °C with 0.5 % skim milk with TBST and *MCM6* (Abcam Cat# ab201683) and *TTK* (Abcam Cat# ab187520) primary antibodies diluted 1:20000 and for 30 min with *TUBA1A* (Abcam Cat# ab7291, RRID:AB_2241126) primary antibodies diluted 1:20000. The solution was then replaced with a new solution of 0.5 % skim milk with TBST and anti-rabbit (Abcam Cat# ab6721, RRID: AB_955447) or anti-mouse (Abcam Cat# ab6789, RRID:AB_955439) secondary antibodies diluted 1:20000 for 30 min. Luminata Forte Western HRP substrate (Thermofisher) was added before imaging.

Western blots were imaged (LAS image) for 20 s, 1 min, or automatic exposure and quantification was performed using ImageJ [36]. *MCM6* and *TTK* expression levels were normalized by dividing by their corresponding α-Tubulin expression levels and each drug treatment expression level was then normalized again by dividing by the mean normalized control expression level.

2.10. Molecular Docking

Molecular docking analyses were performed to comprehend the molecular interaction mechanisms between the target proteins and their correspondingly repositioned drug candidates. 3D-coordinates of the *TTK* protein were retrieved from the protein data bank (PDB ID: 4C4J) while alpha-fold structure of *MCM6* was used [37]. Structures were optimized using quick prep tool of Molecular Operating Environment (MOE, V2019.01) suit to remove gaps, optimize angle, bond length, charges calculation and protonation of amino acids at physiological pH. The structures of the compounds were built using the MOE builder module and was charged and minimized by MMFF94x force field [38]. The standard default docking algorithm and scoring functions (triangle matcher algorithm, London dG and GBVI/WSA) were used. Hundred conformations were generated for each molecule that were analyzed based on clustering. Best suitable docked conformation was selected based on docking scores and interaction profile.

3. Results

3.1. Identification of prognostic genes

We performed the univariate Cox survival analysis based on the gene expression profiles and patients' OS in each cohort. As a result, we identified 1463 unfavorable genes whose high expression was associated with poor survival outcomes of patients and 166 favorable gene whose high expression was associated with good survival outcomes of patients in the TCGA cohort (p-value < 0.01). Similarly, we identified 1111 unfavorable genes and 4 favorable genes in the Uppsala cohort, respectively (p-value < 0.01). We evaluated the concordance of these prognostic genes from the two cohorts and found that these two lists of unfavorable genes have a significant overlap (Fig. 2a, $n = 341$, hypergeometric test, p-value $<$ 1.0E-12). GO enrichment analysis showed that the 341 overlapped unfavorable genes were significantly enriched in chromosome organization and segregation, cell cycle, nuclear division, and DNA replication pathways (Fig. 2b). Similar pathways were observed from the KEGG enrichment analysis (Fig. S1). A significant overlap was also observed between the two lists of favorable genes (Fig. 2a, $n = 3$, hypergeometric test, p-value $<$ 1.0E-12). Since there were only three overlapped favorable genes, *AMPD1*, *JCHAIN*, and *ZNF540*, their functions were examined individually. *AMPD1* encodes adenosine monophosphate deaminase which catalyzes AMP to IMP and it is a crucial enzyme in purine nucleotide and energy metabolism. It has been reported that *AMPD1* expression level is positively correlated to immune cell infiltration level in LUAD [39]. *JCHAIN* encodes immunoglobulin J-chain which is essential in the formation and stabilization of polymeric IgA and IgM structures. The transcription of *JCHAIN* in the lungs substantially decreases during tumorigenesis, which can be explained by the immunosuppressing effect of tumor cells [40]. *ZNF540* acts as a transcriptional repressor, and it is associated with $CD8^+$ T cells infiltrating in LUAD [41].

3.2. Identification of functional modules

We performed Spearman correlation to estimate the association between each two genes based on their gene expression levels in each cohort. The top 1 % of the gene-to-gene links with the highest correlations coefficients were extracted to construct the gene co-expression

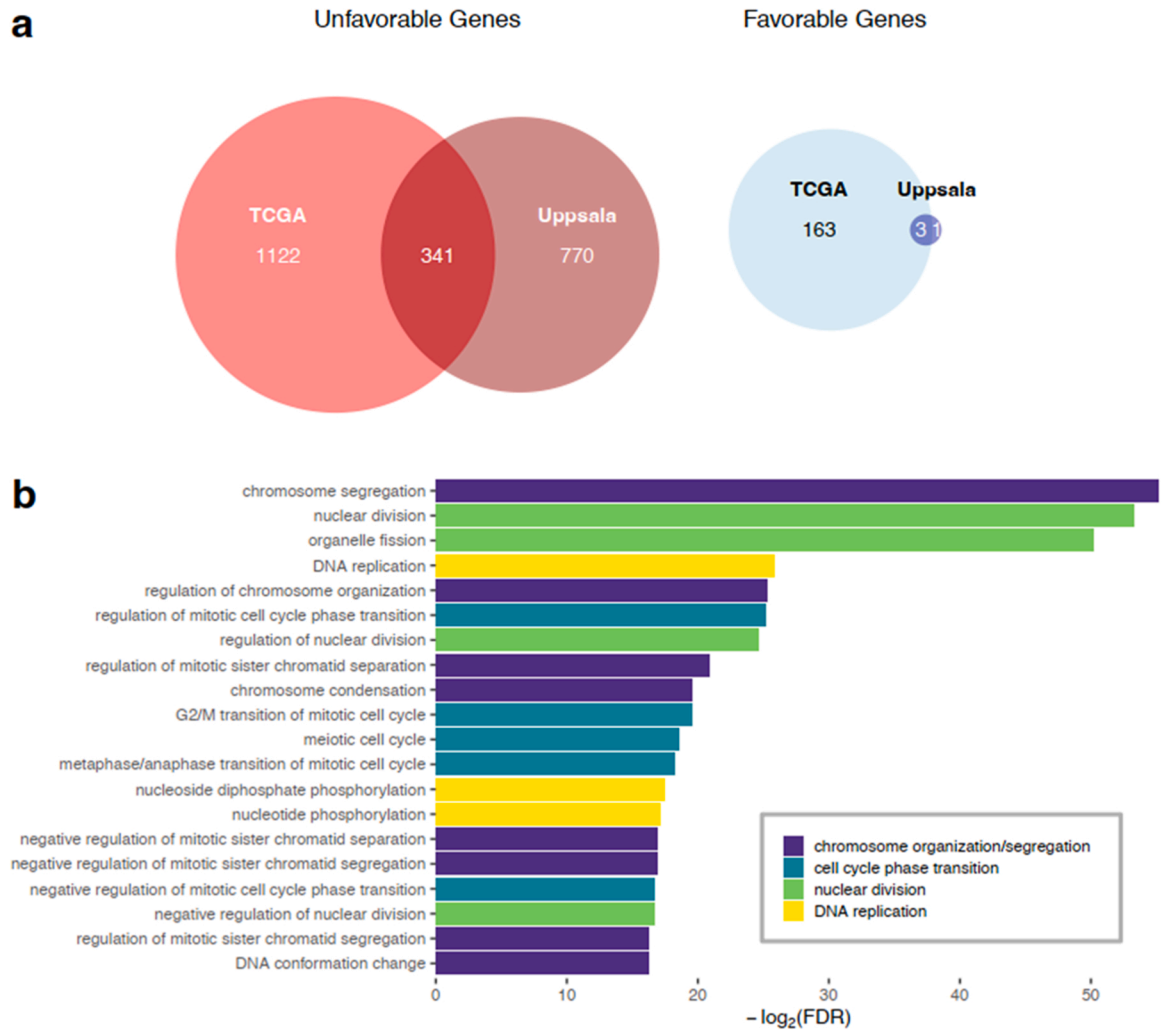

Fig. 2. Identification of prognostic genes. (a) Overlaps of prognostic genes from the two LUAD cohorts. (b) The top 20 most significant GO terms enriched with the 341 overlapped unfavorable genes.

network. We finally obtained around 2,012,288 gene-to-gene links with correlation coefficients ranging from 0.55 to 1 in the gene co-expression network of the TCGA cohort. Further, we used a random walks-based algorithm, Walktrap, to identify the gene modules with high transitivity based on the topology of the CCN [32]. The modules with more than 50 genes and clustering coefficients higher than 0.5 were used for further analysis. In the TCGA gene co-expression network, we identified 14 modules (M1-M14, containing 57–3466 genes) (Fig. 3a). We investigated the association of the modules with the 341 unfavorable genes based on concordance analysis (Table S1). We observed that M3 (455 genes) and M4 (357 genes) had significant overlaps with these unfavorable genes in the TCGA cohort (n = 126 and 20, respectively, hypergeometric test, $p < 0.01$). Thus, these two modules were denoted as unfavorable modules. Functional enrichment showed that the genes involved in M3 were significantly enriched in the chromosome segregation, DNA replication and repair, nuclear division, and cell phase transition related pathways (Table S2). The genes involved in the M4 were significantly enriched in the extracellular organization and angiogenesis pathways (Fig. 3a). We obtained similar pathways by KEGG enrichment analysis (Table S3).

Similarly, we obtained 1979,922 gene-to-gene links with correlation coefficient ranging from 0.57 to 1 in the gene co-expression network of the Uppsala cohort and found 12 modules (M1-M12, containing 51–2664 genes). Among these modules, M4 (391 genes) and M7 (269 genes) had significant overlaps with the unfavorable genes (n = 19 and 99, respectively, hypergeometric test, $p < 0.01$, Table S4). Functional enrichment analysis showed that the two modules exhibited an identical set of GO and KEGG pathways resulting from the TCGA cohort (Fig. 3a, Table S5 and S6). Thus, we inferred that the unfavorable modules identified from the TCGA and Uppsala cohorts were highly consistent. Based on the concordance analysis, we observed that the TCGA M3 had a significant overlap with the Uppsala M7 (n = 242, hypergeometric test: $p < 1.0E\text{-}12$, Jaccard index = 0.5, Table S7). Similar result was observed for the overlaps of TCGA M4 and Uppsala M4 (n = 239, hypergeometric test: $p < 1.0E\text{-}12$, Jaccard index = 0.47, Table S7). These results suggested that the unfavorable modules identified from the TCGA cohort were validated in the independent Uppsala cohort. In addition, a pairwise comparison was performed between the remaining modules identified in the two cohorts. Significant overlaps with high Jaccard indices were also found between TCGA M2 and Uppsala M3 which were enriched in adaptive immune system and cell differentiation pathways, TCGA M5 and Uppsala M8 which were enriched in angiogenesis and blood circulation pathways, TCGA M8 and Uppsala M9 which were enriched for extracellular transport and cilium assembly/organization pathways, and TCGA M11 and Uppsala M10 which were enriched in cytoplasmic translation, ribosome biogenesis, and p53 regulation pathways (Fig. 3b, Table S7).

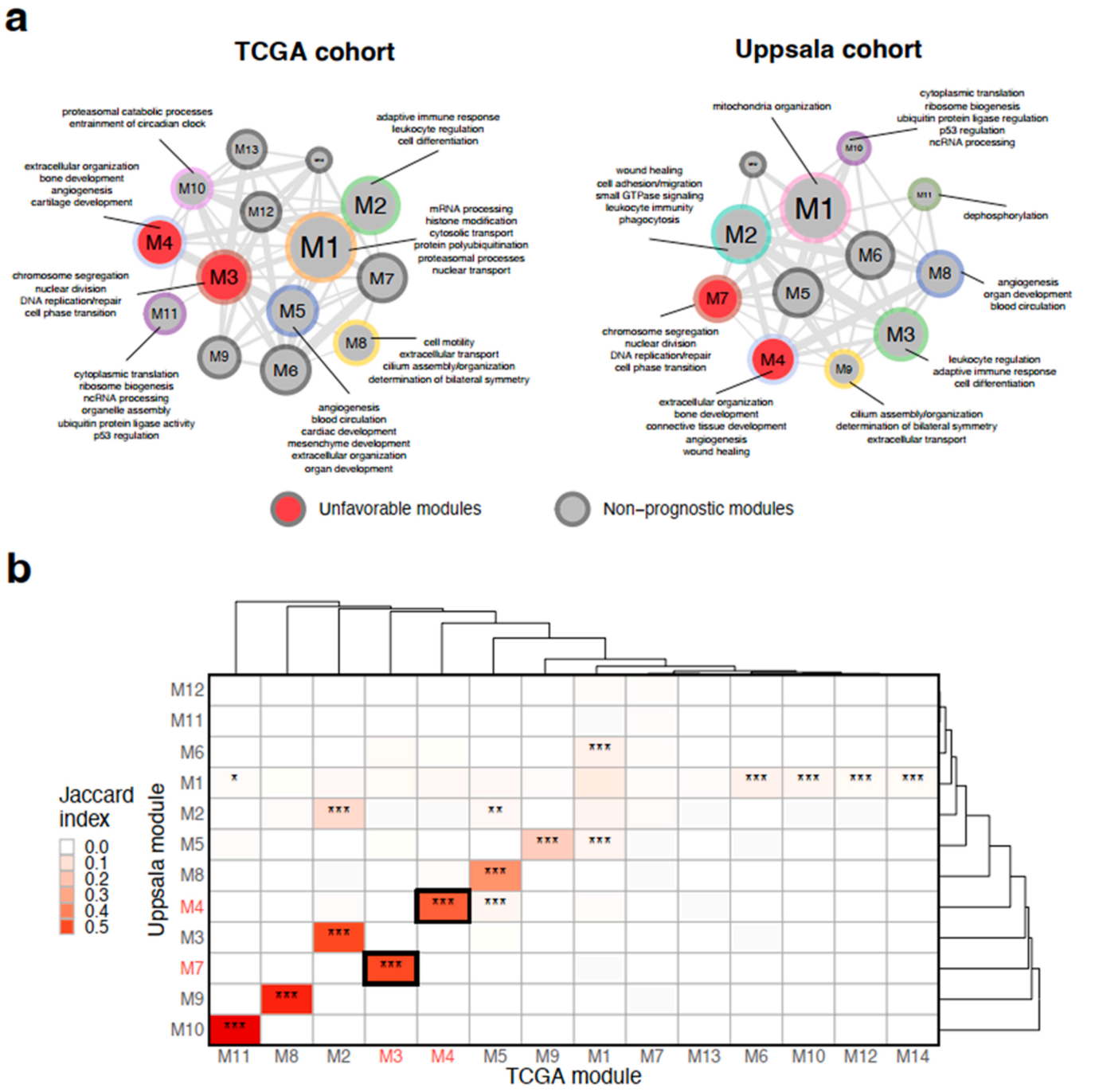

Fig. 3. Identification of functional modules. (a) Functional modules identified from the two cohorts. Module size indicates the number of genes involved in each module. Edge size indicates the number of correlations between genes from each two modules. Red filled module indicates it has a significant overlap with the unfavorable genes. Module border colors highlight different biological functions. Module without any annotation means its involved genes were not significantly enriched in any GO terms (FDR < 0.05). (b) Heatmap showing the overlaps between modules from different cohorts. Unfavorable modules and their overlaps were highlighted with red text and black border. Hypergeometric p-value significance codes: *< 0.05, ** < 0.01, ***< 0.001.

3.3. Identification of targetable genes

To determine the hub genes that might drive the tumor development, we performed topological analysis to estimate the centrality of genes in these unfavorable modules. Degree, closeness and betweenness of genes were evaluated in each module. Then, we calculated the Spearman correlation of each centrality measurement between the pairwise matching of the unfavorable modules from the two cohorts. As a result, the correlation coefficients of degree, closeness and betweenness of genes were 0.86, 0.86 and 0.79 between TCGA M4 and Uppsala M4, and 0.8, 0.8 and 0.58 between TCGA M3 and Uppsala M7 (all p-values < 1.0E-12, Figs. 4a and 4b). Further, we ranked the genes based on a descending order of each centrality measurement in each unfavorable module. The genes ranked within the top 20 in the matching unfavorable modules from the two cohorts were selected as the hub genes. Since the module sizes were 455, 357, 391, 269 for these unfavorable modules TCGA M3, TCGA M4, Uppsala M4 and Uppsala M7, respectively, we selected the top 20 ranking genes to balance the selection sensitivity and bias from different module sizes, and thus controlled the gene selection within the top 10 % (4–7 % in our cases) of genes with highest

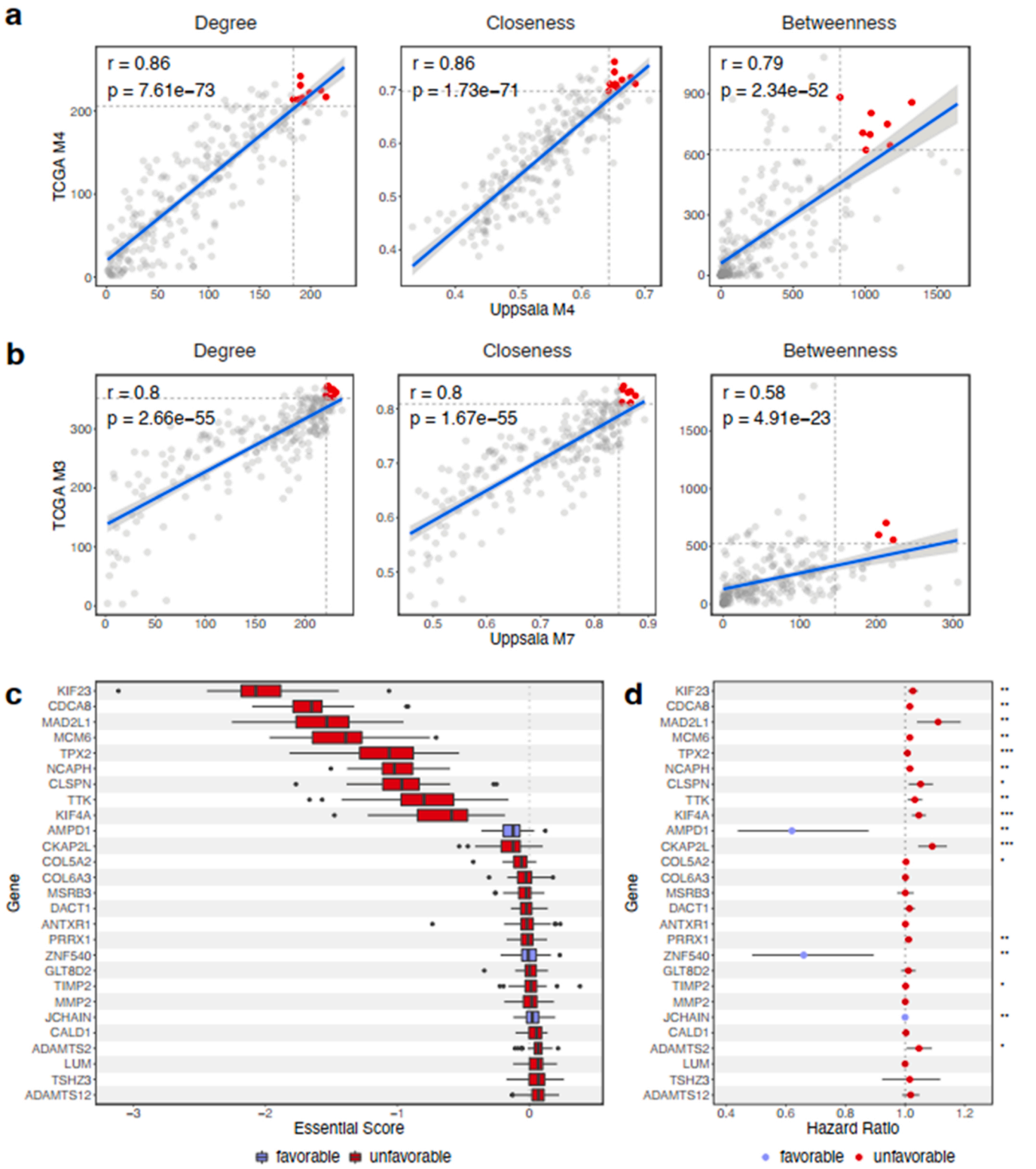

Fig. 4. Identification of the targetable genes. Spearman correlation of centrality measurements (a) between TCGA M4 and Uppsala M4, and (b) between TCGA M3 and Uppsala M7. Each point represents a gene. The genes highlighted by red color indicate that these genes are ranked within the top 20 based on a descending order of the corresponding centrality measurement. The blue lines show a linear fit with the shaded region showing the 95% confidence intervals. In addition, r and p represent the Spearman correlation coefficient and p-value, respectively. (c) Essential scores of the selected genes in 50 LUAD cell lines. (d) Hazard ratios of the selected genes. Lines indicate 95% confidence intervals. Significance levels: * $p < 0.05$, ** $p < 0.01$, *** $p < 0.001$.

centralities in each module. A union set of genes identified based on all the centrality measurements were used as the final hub genes. Totally, 24 hub genes were identified. By including the three overlapped favorable genes, we finally obtained 27 hub genes. Further, we downloaded the essential scores of these genes in 50 LUAD cell lines from the DepMap data portal [34]. The essential score of a gene represents the essentiality of this gene for tumor cell proliferation and survival after knockout of this gene by CRISPR-Cas9 technology. A more negative score indicates worse survival of cells after the gene knockout. As shown in Fig. 4c, nine hub genes, *KIF23*, *CDCA8*, *MAD2L1*, *MCM6*, *TPX2*, *NCAPH*, *CLSPN*, *TTK*, and *KIF4A*, whose essential scores in 50 LUAD cell lines were smaller than 0, were selected as the targetable genes (Fig. 4c). These nine genes were all unfavorable for the patients' prognoses, whose hazard ratios were higher than 1 (Fig. 4d).

3.4. Drug Repositioning

We applied our previously proposed drug repositioning method to identify promising drugs that can have an inhibitory effect on the expression of the targetable genes [15,24]. The algorithm is performed by comparing the similarity of molecular effect on tumor cells perturbed by a drug treatment and a gene knockout. This hypothesizes that a drug is considered to have an inhibitory effect on the expression of a target gene if this drug leads to a wide perturbation on the gene expression landscape in tumor cells which is similar to the effect of the knockout of this target gene (see details in the Method section). Among the nine targetable genes, only three genes *CDCA8*, *MCM6*, and *TTK* had the available transcriptomics signature profiles of two LUAD cell lines A549 and HCC515 that were perturbed by the drug treatment and the corresponding shRNA gene knockout from the LINCS database [42]. In brief, we first constructed the drug-shRNA matrix in which each element represents the similarity of the effect induced by a drug perturbagen and a shRNA gene knockdown perturbagen in each cell line. To maximize the drug treated and genetic perturbed effects, we simplified the drug-shRNA matrix by extracting an optimal dosage/treatment duration for each drug and an optimal shRNA for each gene. Further, we merged the two simplified drug-shRNA matrices from two cell lines by extracting the same drugs. Finally, for each target gene, the top five drugs with the highest mean values of coefficients from two cell lines were selected as the potentially effective drugs (Table S8). Meanwhile, the coefficients in each cell lines should be higher than 0.4. As shown in Fig. 5a, we identified, as top candidate drugs, BRD-K43256821, EMF-BCA1–57, GSK-1059615, curcumin, and alvocidib for inhibiting *CDCA8*, oxetane, mitoxantrone, staurosporine, CGP-60474 and alvocidib for inhibiting *MCM6*, and mitoxantrone, wortmannin and NVP-BEZ235 for inhibiting *TTK*. Among them, only oxetane-containing drugs (*e.g.,* taxol) and mitoxantrone are clinically used drugs, and others are pre-clinical drugs under medical investigation.

3.5. Experimental validation of drug efficacy

Among these repurposed drugs, we were able to obtain only CGP-60474, mitoxantrone, and wortmannin and tested these drugs *in vitro* model A549 cell line. First, we performed dose dependent MTT assays for each drug to select a proper concentration which could reduce the cell viability by 50 %. As a result, 10 μM for CGP-60474, 10 μM for wortmannin and 100 nM for mitoxantrone were determined (Fig. S2). Further, we tested MTT assay for cell viability and LDH assay for cytotoxicity. In MTT assay, cell viability was decreased to 29.1 % ± 0.7 by CGP-60474, 52.2 % ± 1.4 by mitoxantrone and, 62.3 % ± 2.4 by wortmannin (Fig. 5b). Interesting, LDH assays showed that 10 μM CGP-60474 and 10 μM wortmannin did not induce necrotic cell death, and100nM of mitoxantrone showed only 3.45% ± 0.4 necrotic cell death compared to the lysis positive control (100 %) and negative untreated group (0 %) (Fig. 5c). Taken together, cell viability and cytotoxicity assay results indicated that these drugs decreased the cell viability mainly by inhibiting the cell proliferation rather than inducing necrotic cell death procedure. To investigate whether the repurposed drugs could inhibit their corresponding genes we repurposed for, the protein expression levels of these target genes were evaluated in the A549 cell lines after drug treatment. Western blots showed that CGP-60474 and mitoxantrone significantly reduced the protein level of *MCM6* (Fig. 5d and S3). Especially, mitoxantrone showed an extremely effective suppression on *MCM6,* with 95 % decrease of protein expression (Fig. 5d). In addition, mitoxantrone and wortmannin significantly inhibited the protein level of *TTK* by around 50 % (Fig. 5e and S3). Notably, CGP-60474, which was predicted to inhibit *MCM6*, also showed an inhibitory effect on *TTK*. These results suggested that the repurposed drugs effectively targeted the corresponding genes and reduced the tumor cell proliferation.

3.6. Molecular docking

We performed the molecular docking analyses to gain a deep insight of the binding mode between the validated drugs (mitoxantrone, CGP-60474, and wortmannin) and the target proteins (*TTK* and *MCM6*). The predicted docking scores for the binding interactions of mitoxantrone, CGP-60474 and wortmannin against *TTK* were − 9.39, − 8.18 and − 7.28 (kcal/mol), respectively, representing moderate to strong interactions (Table S9). Furthermore, it was observed that there were mostly hydrophilic interactions between the hit compounds and the active site residues of *TTK* (Glu603, Gly605, Ser611, Ala651, Gln671 and Met671) (Fig. 6a), while the aromatic ring of the compounds confers stability by forming hydrophobic interactions with the active site residues (Ile531, Val539, Ala551, Leu654, Ile663 and Asp664). The predicted docking scores for the binding interactions of mitoxantrone and CGP-60474 against *MCM6* were − 7.54 and − 6.37 (kcal/mol), respectively, representing moderate interactions (Table S10). Both drug candidates interacted with crucial residues of the protein by establishing hydrophilic (Gln212, Ala416, Arg217, Lys241, Ser413 and Arg573) and hydrophobic (Gln212, Ala213, Glu410 and Glu411) interaction (Fig. 6b).

4. Discussion

In this study, we employed an integrated approach to identify the therapeutic targets and repurposed the promising drugs for LUAD patients who cannot benefit from the clinically used chemotherapies or targeted therapies. As a result, we identified three druggable gene targets, *CDCA8*, *MCM6* and *TTK*. *CDCA8* encodes a component of the chromosomal passenger complex which is an essential regulator for mitosis and cell division. Supporting to our findings, it has been reported that the phosphorylation and activation of *CDCA8* plays a key role in lung carcinogenesis and the suppression of *CDCA8* significantly inhibits the growth of lung cancer cells [43]. *MCM6* encodes one of the highly conserved mini-chromosome maintenance proteins that are essential for the imitation of eukaryotic genome replication. *MCM6* was involved in the prognostic signatures for indicating the survival outcomes for particularly early-stage LUAD patients [5,6]. *TTK* encodes a dual specificity protein kinase with the ability to phosphorylate tyrosine, serine and threonine, which is a critical mitotic checkpoint protein for accurate segregation of chromosomes during mitosis [44]. It has been reported that *TTK* is overexpressed in tumor tissues compared to normal lung tissue and its selective inhibitor CFI-402257 shows significant antineoplastic activity in LUAD mouse models [45].

Further, we predicted that oxetane, mitoxantrone, staurosporine, CGP-60474 and alvocidib had a potential inhibitory effect on the expression of *MCM6,* and mitoxantrone, wortmannin, and NVP-BEZ235 had a potential inhibitory effect on the expression of *TTK*. Among these drugs, we validated the drug efficacy of mitoxantrone and CGP-60474 for targeting *MCM6*, and mitoxantrone and wortmannin for targeting *TTK* in *in vitro* model. Interestingly, CGP-60474 also suppressed the

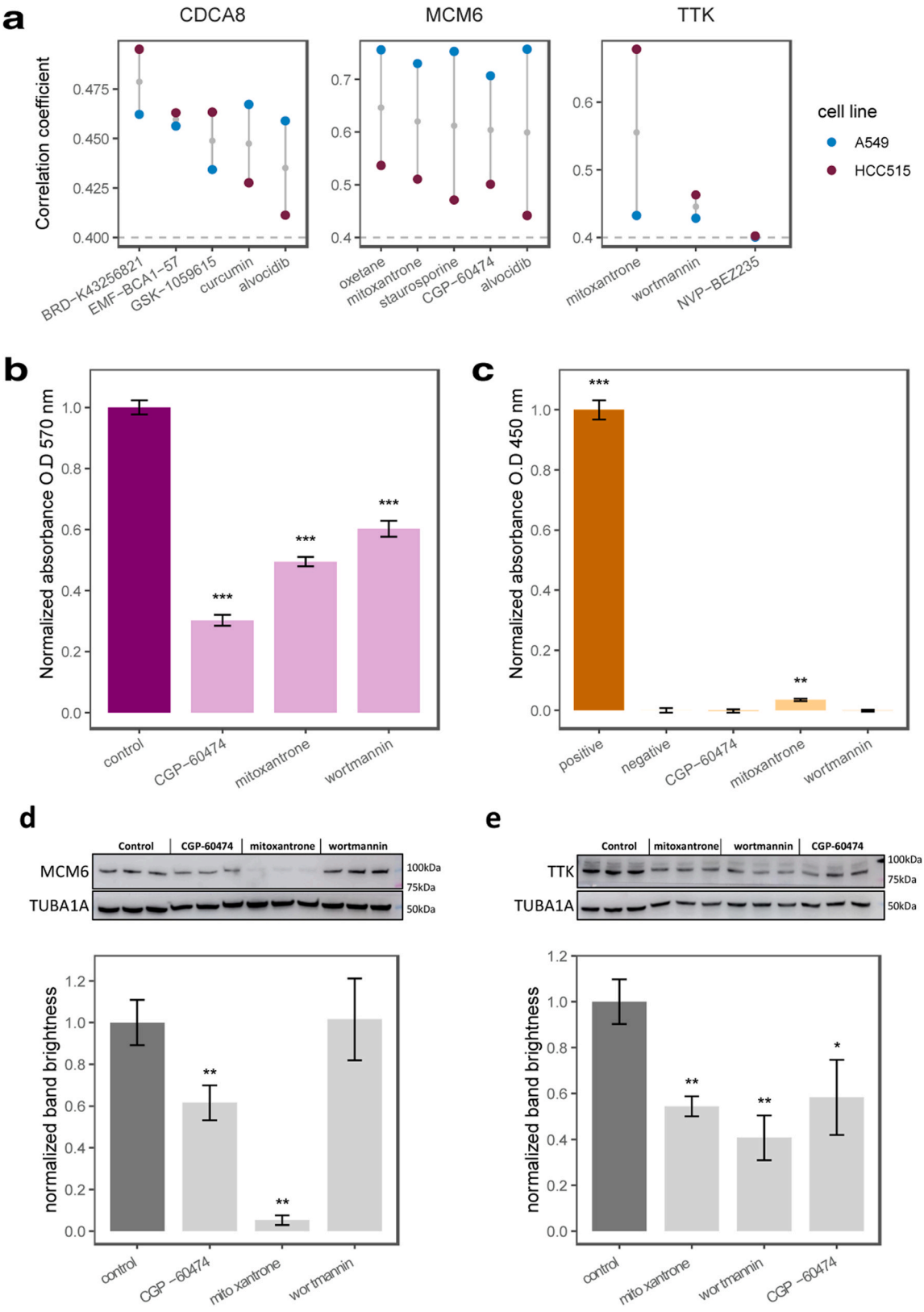

Fig. 5. Drug repositioning and validation of drug efficacy in an *in vitro* model. (a) Correlation coefficients of the top drugs in A549 and HCC515 cell lines. The drug candidates were ranked by the mean values of correlation coefficients from the two cell lines. (b) Bar plot showing the cell viability of A549 cell line after drug treatment in MTT assays. (c) Bar plot showing the cytotoxicity on A549 cell lines after drug treatment in LDH assays. The 'positive' and 'negative' represent the lysis cells and DMSO treated cells, respectively. Difference between groups was estimated by the Student's t-test. Western blots showing the inhibitory effect of drugs on the protein expression of (d) *MCM6* and (e) *TTK*. Error bar represents standard error. Significance levels: * $p < 0.05$, ** $p < 0.01$, *** $p < 0.001$. 10 μM CGP-60474, 10 μM wortmannin and 100 nM mitoxantrone were used for cell treatment.

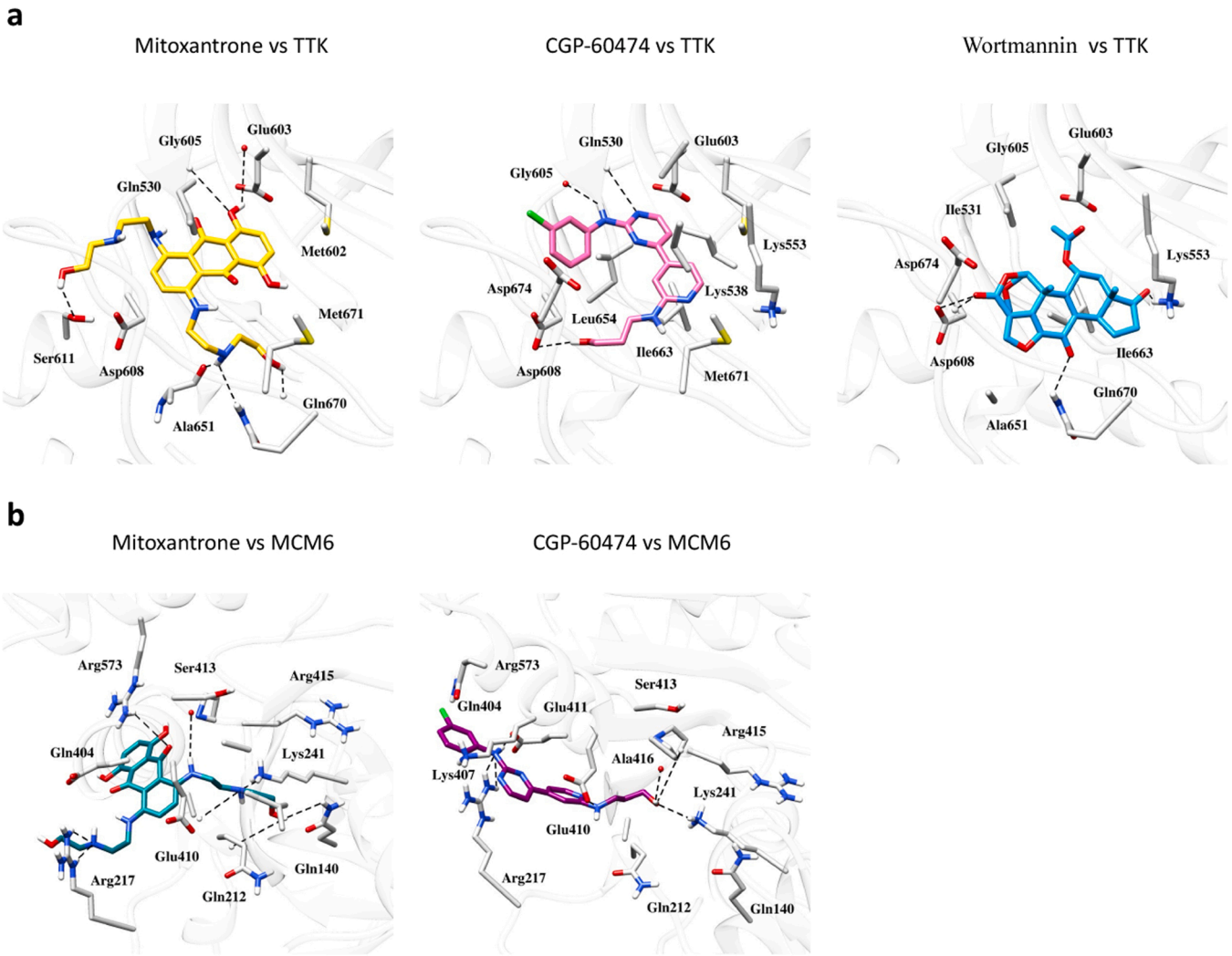

Fig. 6. Molecular docking analysis of predicted drugs and their corresponding targets. (a) Putative binding modes of mitoxantrone, CGP-60474, and wortmannin against *TTK*. (b) Putative binding modes of mitoxantrone and CGP-60474 against *MCM6*. Hydrogen bonds are presented as black dotted lines.

protein level of *TTK*. In the drug repositioning analysis, we set that the correlation coefficient in both lung cancer cell line A549 and HCC515 should be > 0.4 based on previously empirical setting in kidney cancer and liver diseases [15,24,25]. However, we found that the correlation coefficient of interaction between CGP-60474 and *TTK* was 0.3895 in the A549 cell line, which was in the border line but below the cutoff. Thus, unfortunately, we skipped this interaction based on above criterion during the prediction. CGP-60474 is a potent inhibitor of *CDK1* which is one of the cyclin-dependent kinases [46]. Both *CDK1* and *TTK* are involved the control of G1/S and G2/M phases [47,48] and these two genes showed a high correlation in expression across patients from LUAD TCGA cohort in our analysis (Spearman correlation coefficient $= 0.88$), which might explain that CGP-60474 can target *TTK*. Mitoxantrone is an inhibitor of DNA topoisomerase II alpha (*TOP2A*), and it leads to cell deaths by the induction of double stranded DNA breaks [49]. It is currently applied in the treatment of breast and prostate cancers, lymphomas and leukemias. There were two phase II studies that failed to validate the antitumor activity of mitoxantrone in the treatment for lung cancer [50,51]. However, both studies had small sample sizes (each recruited 24 patients), and only advanced or metastatic non-small-cell lung cancer were involved. Based on our analysis, we suggest giving mitoxantrone for the treatment of LUAD patients with early-stage tumors, since its target gene *MCM6* was particularly powerful for the classification of stage I tumors [5,6]. Wortmannin is a fungal metabolite that is identified as a potent and selective inhibitor for phosphoinositide 3-kinases (PI3Ks) [52]. It has been reported that wortmannin inhibits the growth of non-small cell lung cancer in *in vitro* and *in vivo* models [53] and its treatment reverses the cisplatin resistance in lung cancer cells [54].

In this study, we used two different LUAD cohorts in which the patients had different geographic characteristics and cultural backgrounds. Despite these heterogeneities, we found the repeatable prognostic genes, functional gene modules and druggable targets. One limitation of this study is that we might ignore the drugs that do not affect the expression levels of target genes since our method is to check whether the drug perturbation is similar as the target gene knockdown/knockout/overexpression perturbation on human cells.

5. Conclusion

This study demonstrated that our method is feasible in the therapeutic target identification and drug repositioning in LUAD. In this study, we identified nine targetable genes *KIF23*, *CDCA8*, *MAD2L1*, *MCM6*, *TPX2*, *NCAPH*, *CLSPN*, *TTK*, and *KIF4A* that were associated with patients' survival outcomes and found that these genes play a central role in key functional modules, and they are essential for tumor cell growth. Moreover, we repositioned one clinically used drug mitoxantrone, and two pre-clinical drug candidates, including CGP-

60474 and wortmannin, that are promising candidates for the treatment of LUAD patients to modulate *MCM6* or *TTK*. For future work, it is worthwhile to validate the drug efficacy in *in vivo* animal models.

Funding

This research was funded by the National Science Foundation from US (Grant number 1951792) and the Knut and Alice Wallenberg Foundation from Sweden (Grant number: 72254).

CRediT authorship contribution statement

Occam Kelly Graves: Formal analysis, Visualizations, and Writing-original draft. **Woonghee. Kim and Mehmet Özcan**: Validation and Visualization. **Meng Yuan**: Data curation and Resources. **Cheng Zhang**: Data curation and Writing-review&editing. **Adil Mardinoglu**: Supervision, Final acquisition, and Writing-review&editing. **Xiangyu Li**: Project administration, Supervision, Conceptualization, and Writing-review&editing.

Declaration of Interests

X.L. works as a consultant for Bash Biotech Inc., San Diego, CA, USA. A.M. and H.T. are founders and shareholders of Bash Biotech Inc., San Diego, CA, USA. The other authors declare no competing interests.

Data availability

The data availability has been described in the manuscript.

Acknowledgments

Part of computational analysis was performed on the high-performance computing named Uppsala Multidisciplinary Center for Advanced Computational Science (UPPMAX) (under Project SNIC 2022–6-147) which was provided by the Swedish National Infrastructure for Computing (SNIC).

Contributors

O.K.G. contributed to the formal analysis, visualizations, and writing-original draft. W.K. and M.Ö. contributed to the *in vitro* experimental validation and visualization. S.A. and H.Z. contributed to the formal analysis and visualization. M.Y. contributed to the data curation and resources. C.Z. contributed to project administration, data curation, writing-review&editing. A.M. contributed to the supervision, final acquisition, and writing-review&editing. X.L. contributed to the project administration, supervision, conceptualization, and writing-review&editing. All the authors read and approved the final manuscript.

Appendix A. Supporting information

Supplementary data associated with this article can be found in the online version at doi:10.1016/j.biopha.2023.114486.

References

[1] H. Sung, J. Ferlay, R.L. Siegel, et al., Global cancer statistics 2020: GLOBOCAN estimates of incidence and mortality worldwide for 36 cancers in 185 countries, Cancer J. Clin. 71 (3) (2021) (209-49).
[2] S.J. Behrend, G.A. Giotopoulou, M. Spella, G.T. Stathopoulos, A role for club cells in smoking-associated lung adenocarcinoma, Eur. Respir. Rev. 30 (2021) 162.
[3] D.S. Ettinger, D.E. Wood, D.L. Aisner, et al., Non-small cell lung cancer, Version 3.2022, NCCN clinical practice guidelines in oncology, J. Natl. Compr. Cancer Netw. 20 (5) (2022) 497–530.
[4] F.R. Hirsch, G.V. Scagliotti, J.L. Mulshine, et al., Lung cancer: current therapies and new targeted treatments, Lancet 389 (10066) (2017) 299–311.
[5] V. Melocchi, E. Dama, F. Mazzarelli, et al., Aggressive early-stage lung adenocarcinoma is characterized by epithelial cell plasticity with acquirement of stem-like traits and immune evasion phenotype, Oncogene 40 (31) (2021), 4980-91.
[6] H. Kadara, C. Behrens, P. Yuan, et al., A five-gene and corresponding protein signature for stage-I lung adenocarcinoma prognosis, Clin. Cancer Res. 17 (6) (2011) 1490–1501.
[7] Z. Feng, Y. Zhang, M. He, et al., AMICA1 is a diagnostic and prognostic biomarker and induces immune cells infiltration by activating cGAS-STING signaling in lung adenocarcinoma, Cancer Cell Int. 22 (1) (2022) 111.
[8] M. He, Y. Han, C. Cai, et al., CLEC10A is a prognostic biomarker and correlated with clinical pathologic features and immune infiltrates in lung adenocarcinoma, J. Cell Mol. Med. 25 (7) (2021) 3391–3399.
[9] X.S. Liu, L.M. Zhou, L.L. Yuan, et al., NPM1 is a prognostic biomarker involved in immune infiltration of lung adenocarcinoma and associated with m6A modification and glycolysis, Front. Immunol. 12 (2021), 724741.
[10] Y. He, R. Liu, M. Yang, et al., Identification of VWF as a novel biomarker in lung adenocarcinoma by comprehensive analysis, Front. Oncol. 11 (2021), 639600.
[11] M. Lu, X. Fan, W. Liao, et al., Identification of significant genes as prognostic markers and potential tumor suppressors in lung adenocarcinoma via bioinformatical analysis, BMC Cancer 21 (1) (2021) 616.
[12] T. Bian, M. Zheng, D. Jiang, et al., Prognostic biomarker TUBA1C is correlated to immune cell infiltration in the tumor microenvironment of lung adenocarcinoma, Cancer Cell Int. 21 (1) (2021) 144.
[13] Z. Jiawei, M. Min, X. Yingru, et al., Identification of key genes in lung adenocarcinoma and establishment of prognostic mode, Front. Mol. Biosci. 7 (2020), 561456.
[14] S. Pushpakom, F. Iorio, P.A. Eyers, et al., Drug repurposing: progress, challenges and recommendations, Nat. Rev. Drug Discov. 18 (1) (2019) 41–58.
[15] X. Li, K. Shong, W. Kim, et al., Prediction of drug candidates for clear cell renal cell carcinoma using a systems biology-based drug repositioning approach, EBioMedicine 78 (2022), 103963.
[16] J. Lamb, E.D. Crawford, D. Peck, et al., The Connectivity Map: using gene-expression signatures to connect small molecules, genes, and disease, Science 313 (5795) (2006) 1929–1935.
[17] M. Iskar, M. Campillos, M. Kuhn, L.J. Jensen, V. van Noort, P. Bork, Drug-induced regulation of target expression, PLOS Comput. Biol. 6 (2010) 9.
[18] A.B. Nagaraj, Q.Q. Wang, P. Joseph, et al., Using a novel computational drug-repositioning approach (DrugPredict) to rapidly identify potent drug candidates for cancer treatment, Oncogene 37 (3) (2018) 403–414.
[19] T. Pillaiyar, S. Meenakshisundaram, M. Manickam, M. Sankaranarayanan, A medicinal chemistry perspective of drug repositioning: recent advances and challenges in drug discovery, Eur. J. Med. Chem. 195 (2020), 112275.
[20] G. Jin, S.T. Wong, Toward better drug repositioning: prioritizing and integrating existing methods into efficient pipelines, Drug Discov. Today 19 (5) (2014) 637–644.
[21] R.X. Huang, D. Siriwanna, W.C. Cho, et al., Lung adenocarcinoma-related target gene prediction and drug repositioning, Front. Pharmacol. 13 (2022), 936758.
[22] M.A. De Bastiani, F. Klamt, Integrated transcriptomics reveals master regulators of lung adenocarcinoma and novel repositioning of drug candidates, Cancer Med. 8 (15) (2019) 6717–6729.
[23] O.S. Kwon, H. Lee, H.J. Kong, et al., Connectivity map-based drug repositioning of bortezomib to reverse the metastatic effect of GALNT14 in lung cancer, Oncogene 39 (23) (2020) 4567–4580.
[24] C. Zhang, M. Shi, W. Kim, et al., Discovery of therapeutic agents targeting PKLR for NAFLD using drug repositioning, EBioMedicine 83 (2022), 104214.
[25] M. Yuan, K. Shong, X. Li, et al., A gene Co-expression network-based drug repositioning approach identifies candidates for treatment of hepatocellular carcinoma, Cancers 14 (6) (2022).
[26] Cancer Genome Atlas Research N, Comprehensive molecular profiling of lung adenocarcinoma, Nature 511 (7511) (2014) 543–550.
[27] A. Mezheyeuski, C.H. Bergsland, M. Backman, et al., Multispectral imaging for quantitative and compartment-specific immune infiltrates reveals distinct immune profiles that classify lung cancer patients, J. Pathol. 244 (4) (2018) 421–431.
[28] T. Goldmann, S. Marwitz, D. Nitschkowski, et al., PD-L1 amplification is associated with an immune cell rich phenotype in squamous cell cancer of the lung, Cancer Immunol. Immunother. 70 (9) (2021) 2577–2587.
[29] N.L. Bray, H. Pimentel, P. Melsted, L. Pachter, Erratum: Near-optimal probabilistic RNA-seq quantification, in: Nat Biotechnol, 34, 2016, p. 888.
[30] Therneau T., Lumley T.R. survival package. R Core Team 2013.
[31] G. Yu, L.G. Wang, Y. Han, Q.Y. He, clusterProfiler: an R package for comparing biological themes among gene clusters, OMICS 16 (5) (2012) 284–287.
[32] Pons P., Latapy M. Computing communities in large networks using random walks. In: Proceedings of the International Symposium on Computer and Information Sciences 2005; 3733: 284–293.
[33] M. Nascimento, A. Carvalho, A graph clustering algorithm based on a clustering coefficient for weighted graphs, J. Braz. Comput. Soc. 17 (2011) 19.
[34] R.M. Meyers, J.G. Bryan, J.M. McFarland, et al., Computational correction of copy number effect improves specificity of CRISPR-Cas9 essentiality screens in cancer cells, Nat. Genet. 49 (12) (2017) 1779–1784.
[35] A. Subramanian, R. Narayan, S.M. Corsello, et al., A next generation connectivity map: L1000 platform and the first 1,000,000 profiles, Cell 171 (6) (2017) 1437–1452.
[36] C.A. Schneider, W.S. Rasband, K.W. Eliceiri, NIH Image to ImageJ: 25 years of image analysis, Nat. Methods 9 (7) (2012) 671–675.

[37] S. Naud, I.M. Westwood, A. Faisal, et al., Structure-based design of orally bioavailable 1H-pyrrolo[3,2-c]pyridine inhibitors of mitotic kinase monopolar spindle 1 (MPS1), J. Med. Chem. 56 (24) (2013) 10045–10065.
[38] T.A. Halgren, Merck molecular force field. I. Basis, form, scope, parameterization, and performance of MMFF94, J. Comput. Chem. 17 (1996) 490.
[39] Z.Y. Xu, M. Zhao, W. Chen, et al., Analysis of prognostic genes in the tumor microenvironment of lung adenocarcinoma, PeerJ 8 (2020), e9530.
[40] D.K. Slizhikova, M.V. Zinov'eva, D.V. Kuz'min, et al., [Decrease in expression of human J-chain in lung squamous cell cancer and adenocarcinoma], Mol. Biol. 41 (4) (2007) 659–665.
[41] M. Zhang, J. Ma, Q. Guo, S. Ding, Y. Wang, H. Pu, CD8(+) T cell-associated gene signature correlates with prognosis risk and immunotherapy response in patients with lung adenocarcinoma, Front. Immunol. 13 (2022), 806877.
[42] V. Stathias, J. Turner, A. Koleti, et al., LINCS data portal 2.0: next generation access point for perturbation-response signatures, Nucleic Acids Res. 48 (D1) (2020) D431–D439.
[43] S. Hayama, Y. Daigo, T. Yamabuki, et al., Phosphorylation and activation of cell division cycle associated 8 by aurora kinase B plays a significant role in human lung carcinogenesis, Cancer Res. 67 (9) (2007) 4113–4122.
[44] E. Lauze, B. Stoelcker, F.C. Luca, E. Weiss, A.R. Schutz, M. Winey, Yeast spindle pole body duplication gene MPS1 encodes an essential dual specificity protein kinase, EMBO J. 14 (8) (1995) 1655–1663.
[45] L. Zheng, Z. Chen, M. Kawakami, et al., Tyrosine threonine kinase inhibition eliminates lung cancers by augmenting apoptosis and polyploidy, Mol. Cancer Ther. 18 (10) (2019) 1775–1786.
[46] P. Furet, J. Zimmermann, H.G. Capraro, T. Meyer, P. Imbach, Structure-based design of potent CDK1 inhibitors derived from olomoucine, J. Comput. Aided Mol. Des. 14 (5) (2000) 403–409.
[47] D. Hogg, C. Guidos, D. Bailey, et al., Cell cycle dependent regulation of the protein kinase TTK, Oncogene 9 (1) (1994) 89–96.
[48] T. Bashir, M. Pagano, Cdk1: the dominant sibling of Cdk2, Nat. Cell Biol. 7 (8) (2005) 779–781.
[49] B.J. Evison, B.E. Sleebs, K.G. Watson, D.R. Phillips, S.M. Cutts, Mitoxantrone, More than just another topoisomerase II poison, Med. Res. Rev. 36 (2) (2016) 248–299.
[50] J. Suga, N. Saijo, T. Shinkai, et al., Phase II study of mitoxantrone in patients with non-small cell lung cancer, Jpn J. Clin. Oncol. 16 (2) (1986) 147–151.
[51] L.G. Feun, N. Savaraj, J. Solomon, A. Liebmann, J. Hurley, Phase II trial of mitoxantrone and cisplatin in advanced non-small-cell lung cancer, Am. J. Clin. Oncol. 19 (2) (1996) 190–192.
[52] G. Powis, R. Bonjouklian, M.M. Berggren, et al., Wortmannin, a potent and selective inhibitor of phosphatidylinositol-3-kinase, Cancer Res. 54 (9) (1994) 2419–2423.
[53] A.S. Boehle, R. Kurdow, L. Boenicke, et al., Wortmannin inhibits growth of human non-small-cell lung cancer in vitro and in vivo, Lange Arch. Surg. 387 (5–6) (2002) 234–239.
[54] Y. Zhang, C. Bao, Q. Mu, et al., Reversal of cisplatin resistance by inhibiting PI3K/Akt signal pathway in human lung cancer cells, Neoplasma 63 (3) (2016) 362–370.